



HAL
open science

Initiation of edge debonding: coupled criterion versus cohesive zone model

Eric Martin, Thomas Vandellos, Dominique Leguillon, Nicolas Carrère

► **To cite this version:**

Eric Martin, Thomas Vandellos, Dominique Leguillon, Nicolas Carrère. Initiation of edge debonding: coupled criterion versus cohesive zone model. *International Journal of Fracture*, 2016, 199 (2), pp.157-168. 10.1007/s10704-016-0101-2 . hal-04776491

HAL Id: hal-04776491

<https://hal.science/hal-04776491v1>

Submitted on 11 Nov 2024

HAL is a multi-disciplinary open access archive for the deposit and dissemination of scientific research documents, whether they are published or not. The documents may come from teaching and research institutions in France or abroad, or from public or private research centers.

L'archive ouverte pluridisciplinaire **HAL**, est destinée au dépôt et à la diffusion de documents scientifiques de niveau recherche, publiés ou non, émanant des établissements d'enseignement et de recherche français ou étrangers, des laboratoires publics ou privés.



Distributed under a Creative Commons Attribution - NonCommercial 4.0 International License

Initiation of edge debonding: coupled criterion versus cohesive zone model

Eric Martin, Thomas Vandellos,
Dominique Leguillon, Nicolas Carrère

Abstract Cohesive zone models and criteria based on finite fracture mechanics are two alternatives to analyze edge debonding. A comparison between the two approaches is presented in this paper. The coupled criterion which combines a stress and an energy conditions to estimate crack initiation is used and compared with a bilinear cohesive law. Predictions of the debonding onset are in good agreement provided the characteristic fracture length of the interface remains smaller than the characteristic dimension of the specimen.

Keywords Crack initiation · Coupled criterion · Debonding · Brittle fracture

1 Introduction

Bonded joints are employed in various engineering fields as an efficient process to join components (Adams and Wake 1984). Among the various techniques available for the strength prediction of bonded joints, one may find stress approaches which compare maximum stresses with material strength or energy approaches which rely on linear elastic fracture mechanics and assume the existence of an initial flaw (Da Silva and Campilho 2012). To predict accurately crack initiation within the bonded area, other approaches are needed.

Based on damage mechanics, cohesive zone models (CZM) describe the traction separation behavior of interfaces using a softening law which can be distinguished by three parts: (1) the increase of the traction until a peak value, which may correspond to an elastic undamaged behavior, (2) the decrease of the traction as a consequence of the development of interfacial damage which induces the loss of the interfacial stiffness of the cohesive element and (3) the apparition of traction-free surfaces when the traction attains the zero value. Following the first papers of (Barenblatt 1959) and (Dugdale 1960), CZM (Tvergaard and Hutchinson 1992; Xu and Needleman 1994) have been extensively used in the literature to analyze the fracture of inter-

E. Martin (✉)
Laboratoire des Composites Thermo-Structuraux CNRS
UMR 5801, Université Bordeaux, 3 rue La Boétie,
33600 PESSAC, France
e-mail: martin@lcts.u-bordeaux1.fr

T. Vandellos
ONERA, 92322 Châtillon Cedex, France

Present address:
T. Vandellos
Herakles Le Haillan, 33185 Le Haillan, France
e-mail: thomas.vandellos@herakles.com

D. Leguillon
Institut Jean Le Rond d'Alembert CNRS UMR 7190,
Université Pierre et Marie Curie, 4 place Jussieu,
75005 Paris, France
e-mail: dominique.leguillon@upmc.fr

N. Carrère
LBMS, ENSTA Bretagne, Université Brest, Brest, France
e-mail: nicolas.carrere@ensta-bretagne.fr

faces in various material systems including delamination in composite laminates (Allix and Ladeveze 1992; Corigliano 1993; Schellekens and Borst 1993; Allix and Corigliano 1996; Turon et al. 2010) and bonded joints (Liljedahl et al. 2006; Gustafson and Waas 2009; Campilho et al. 2012).

Linear elastic fracture mechanics analyzes crack growth in brittle materials but fails to predict crack initiation. For this purpose, finite fracture mechanics is convenient as it allows to consider finite crack increment (Hashin 1996; Nairn 2000). As shown by Leguillon (2002), combining stress and energy conditions provides the applied loading and the crack increment size at crack initiation. This coupled criterion (CC) has recently been demonstrated successful to solve various problems enclosing crack interaction with an interface (Mantič 2009; Leguillon and Martin 2012; García et al. 2014, 2015), edge cracking (Martin et al. 2010; Leguillon et al. 2015), notched strength (Carpinteri et al. 2008; Hebel et al. 2010; Martin et al. 2012; Sapora et al. 2013) and bond strength (Weißgraeber and Becker 2013; Hell et al. 2014; Carrère et al. 2015).

The aim of this paper is to compare the ability of these two approaches to predict the initiation of interfacial debonding. The selected geometry is a bimaterial specimen submitted to a four-point bending test (Fig. 1a). It is assumed that edge debonding (e.g. debonding failure starts from the ends of the sample as illustrated in Fig. 1b) is the dominant failure mechanism which results from the concentration of interfacial stresses. This testing geometry may be used to characterize adhesive joints (Cotton et al. 2001; Leguillon et al. 2003) and metal-ceramic bonds (Lenz et al. 1995) or to analyze the debonding of stiffeners for aeronautic components (Bertolini et al. 2009) and of reinforcing plates for civil engineering structures (Lorenzis and Zavarise 2009; Cornetti et al. 2015). This paper is the main part of a study on edge debonding which has been completed by other contributions concerning the comparison of various shapes of the cohesive law (Vandellos et al. 2014), the use of a strain energy criterion (Martin and Leguillon 2015) and the analysis of substrate cracking in the vicinity of the edge (Martin et al. 2014). The paper is organized as follows: the CC is outlined in Sect. 2, Section 3 describes briefly the CZM and a comparison between both methods with an experimental result is presented in Sect. 4.

The geometrical parameters reported in Fig. 1 are fixed to be $\ell = 20$ mm, $L_1 = 25$ mm and $L_2 = 40$ mm.

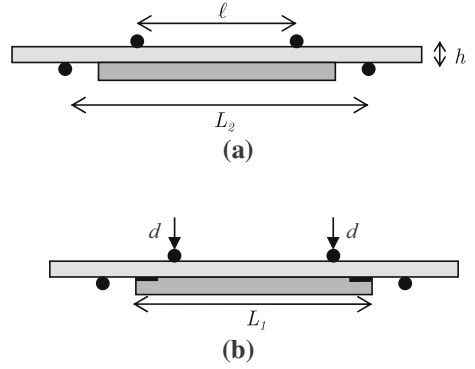


Fig. 1 The bimaterial specimen: **a** geometry of the four-point bending test, **b** initiation of edge debonding upon loading

The substrates have the same thickness $h = 2$ mm and the same elastic properties (Young's modulus $E_s = 400$ GPa and Poisson's ratio $\nu_s = 0.2$). The thickness of the bonding interlayer is first neglected. The sample is submitted to a monotonic increasing displacement d .

2 Coupled criterion

Within the framework of finite fracture mechanics (Hashin 1996), crack initiation in the vicinity of a stress concentration point is the formation of a crack with a finite area ΔA . The incremental energy criterion is defined by

$$-\Delta W \geq G^c \Delta A, \quad (1)$$

where $-\Delta W = W(0) - W(A)$ denotes the decrease of the potential energy and $G^c \Delta A$ (where G^c is the fracture toughness) is the energy dissipated during the crack onset. For a 2D analysis the crack area is given by $\Delta A = ba$ where a is the crack increment length and b is the sample width. The energy condition can also be written as

$$G^{inc}(a) \geq G^c, \quad (2)$$

which introduces the incremental energy release rate defined by $G^{inc}(a) = -\frac{1}{b} \frac{\Delta W}{a}$. This parameter must be distinguished from the differential energy release rate $G(a) = -\frac{1}{b} \frac{dW}{da}$ which enters the formulation of the classical Griffith criterion. As established by Martin and Leguillon (2004), the relationship between $G(a)$ and $G^{inc}(a)$ is

$$G^{inc}(a) = \frac{1}{a} \int_0^a G(\ell) d\ell. \quad (3)$$

To determine the crack size at initiation, an additional condition is needed. Leguillon (2002) proposed to use a stress condition which states that the opening normal stress σ_{op} along the expected crack surface S must exceed the tensile strength σ^c with

$$\sigma_{op}(M) \geq \sigma^c, \quad \forall M \in S. \quad (4)$$

Relations (2) and (4) define the coupled criterion for crack initiation. As shown by Leguillon (2002), $G^{inc}(a)$ is usually an increasing function of the crack length. Fulfilling the inequality (2) implies a crack jump at onset and defines a lower bound of admissible crack lengths. This lower bound decreases with the applied load. Similarly, the stress σ_{op} is a decreasing function of the potential crack length and the second inequality (4) provides an upper bound of admissible crack lengths. This upper bound increases with the applied load. Combining (2) and (4) supplies a unique crack length and the lowest loading at crack onset. This approach naturally introduces a characteristic fracture length $E_s \frac{G^c}{(\sigma^c)^2}$ to derive the crack length at initiation. The next section formulates the coupled criterion with the help of a two-dimensional analysis of the edge debonding applied to the selected bimaterial specimen.

2.1 Formulation

Although the normal opening stress is prevailing in the vicinity of the edge, a stress analysis reveals the presence of shear along the interface. Following the proposal of García and Leguillon (2012), the stress condition is written

$$\sqrt{\left(\frac{\sigma_{yy}(x, y=0)}{\sigma_i^c}\right)^2 + \left(\frac{\sigma_{xy}(x, y=0)}{\tau_i^c}\right)^2} \geq 1, \quad \forall x \leq a, \quad (5)$$

where σ_{yy} and σ_{xy} are respectively the interfacial opening and shear stresses, σ_i^c and τ_i^c are respectively the interfacial tensile and shear strengths. The coordinates (x, y) are indicated in Fig. 2. To take into account the influence of mode mix on the dissipated energy, the energy condition is written

$$G_i^{inc}(a) \geq \frac{1}{a} \int_0^a G_i^c(\psi(x)) dx, \quad (6)$$

where the index i holds for interface. The mode mix $\psi(x)$ is obtained with the help of the stress state prior to the crack onset (García and Leguillon 2012) with

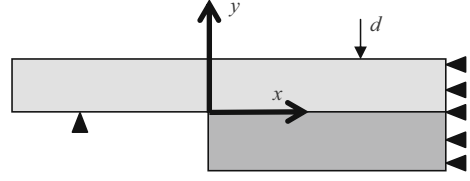


Fig. 2 Geometry of the two-dimensional model used to obtain the numerical results

$$\psi(x) = \tan^{-1} \left(\frac{\sigma_{xy}(x)}{\sigma_{yy}(x)} \right). \quad (7)$$

The main difficulty lies in the definition of $G_i^c(\psi)$ which relies on empirical laws which are difficult to identify (Banks-Sills 2015). In order to facilitate the comparison between CC and CZM, the influence of mode mix is not considered by assuming that $\tau_i^c = \sigma_i^c$ and that $G_i^c(\psi) = G_i^c$. The stress condition (5) can be expressed as

$$\sigma_{eq}(x) = \sqrt{\sigma_{yy}^2(x) + \sigma_{xy}^2(x)} \geq \sigma_i^c, \quad \forall x \leq a. \quad (8)$$

The equivalent stress σ_{eq} is linearly related to the applied displacement d with $\sigma_{eq}(x) = E_i k_{eq}(x) \left(\frac{d}{h}\right)$ which introduces a dimensionless coefficient $k_{eq}(x)$ and the plane strain modulus $E_i = \frac{E_s}{1-\nu_s^2}$. The incremental energy release rate which depends on the square of the loading can be written as

$$G_i^{inc}(a) = E_i h \bar{A}_i(a) \left(\frac{d}{h}\right)^2, \quad (9)$$

where $\bar{A}_i(a)$ is a dimensionless coefficient and h is the thickness of the substrate as shown in Fig. 1.

Coefficients $\bar{A}_i(a)$ and $k_{eq}(x)$ are estimated with the help of an elastic finite element analysis. A two-dimensional model is used to perform elastic calculations assuming a plane strain state. Only one half of the sample is meshed and the boundary conditions are prescribed displacements as illustrated in Fig. 2. The mesh is highly refined near the edge with an element size L_{mesh} smaller than $0.08h$ over an area larger than $50L_{mesh}$ by $50L_{mesh}$. Interfacial nodes are unbuttoned to introduce a crack increment of length a and $\bar{A}_i(a)$ is obtained by $\bar{A}_i(a) = \frac{\Delta W}{a E_i h \left(\frac{d}{h}\right)^2}$ where

$\Delta W = W(a=0) - W(a)$ is the change in elastic energy induced by crack initiation. Numerical results confirm that $k_{eq}(x)$ is a decreasing function but also reveal that $\bar{A}_i(a)$ is not a monotonic function (Fig. 3) and exhibits a maximum value for $a = a^{max}$. A similar

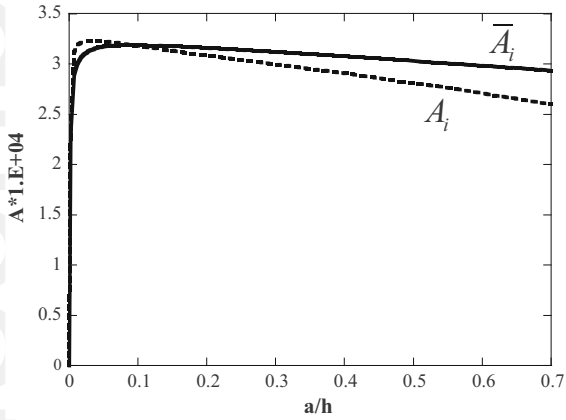


Fig. 3 Dimensionless incremental ($\bar{A}_i(a)$) and differential ($A_i(a)$) energy release rates versus the dimensionless crack length. The incremental energy release rate is maximum for $a = a^{\max} = 0.09h$ and the property $\bar{A}_i(a^{\max}) = A_i(a^{\max})$ is observed and can be proved (Martin and Leguillon 2004)

non-monotonic behavior is also reported for different geometries involved in the analysis of free edge delamination (Martin et al. 2010) or transverse cracking (García et al. 2014) in composite laminates or debonding at the fiber/matrix interface in composite materials (Martin et al. 2008). A more complex behavior showing the presence of a local maximum followed by a local minimum is demonstrated for the single lap joint geometry (Hell et al. 2014; Carrère et al. 2015).

As a consequence of the existence of this maximum and for a monotonically increasing displacement, the energy condition (2) will be first met for $a = a^{\max}$ if

$$G_i^{\text{inc}}(a^{\max}) = E_i h \bar{A}_i(a^{\max}) \left(\frac{d}{h}\right)^2 = G_i^c. \quad (10)$$

In order to fulfill the coupled criterion, the stress condition (8) must also be satisfied with

$$\sigma_{eq}(x) = E_i k_{eq}(x) \left(\frac{d}{h}\right) \geq \sigma_i^c, \quad \forall x \leq a^{\max}. \quad (11)$$

Combining (10) and (11) (and reminding that $k_{eq}(x)$ is a decreasing function) leads to the condition

$$E_i \frac{G_i^c}{(\sigma_i^c)^2} \geq \frac{\bar{A}_i(a^{\max})}{[k_{eq}(a^{\max})]^2} h, \quad (12)$$

which involves the structural length $L_i^{\max} = \frac{\bar{A}_i(a^{\max})}{[k_{eq}(a^{\max})]^2} h$ and the length $L_i^c = E_i \frac{G_i^c}{(\sigma_i^c)^2}$ which is a characteristic fracture length of the interface. If the

characteristic length is large enough to satisfy (12), the energy condition is governing since the stress condition holds true. In this case, the crack length at initiation is $a^* = a^{\max}$ and the corresponding applied displacement is given by $d^* = h \sqrt{\frac{G_i^c}{E_i h \bar{A}_i(a^{\max})}}$ which only depends on G_i^c . If condition (11) is not met, the applied displacement must be increased and the energy condition $E_i h \bar{A}_i(a) \left(\frac{d}{h}\right)^2 = G_i^c$ will be satisfied for $a < a^{\max}$. Combining with the stress condition $E_i k_{eq}(x) \left(\frac{d}{h}\right) = \sigma_i^c$ leads to the estimation of the crack length at initiation a^* with

$$\frac{\bar{A}_i(a^*)}{k_{eq}(a^*)^2} = \frac{L_i^c}{h}. \quad (13)$$

Relation (13) can also be written $\frac{\sqrt{\bar{A}_i(a^*)}}{k_{eq}(a^*)} = \sqrt{\frac{L_i^c}{h}}$

where $\sqrt{\frac{L_i^c}{h}}$ is a dimensionless number similar to the brittleness number introduced by Mantič (2009) as a generalization of Carpinteri's brittleness number (Carpinteri 1982) to interfacial cracks. Solving (13) is always possible as its left hand side is an increasing function of a^* vanishing for $a^* = 0$. Then the displacement at initiation is given by $d^* = h \sqrt{\frac{G_i^c}{E_i h \bar{A}_i(a^*)}} = h \frac{\sigma_i^c}{E_i k_{eq}(a^*)}$ which now depends on G_i^c and σ_i^c . The solution provided by the CC can be summarized in

$$\begin{cases} L_i^c < L_i^{\max}, a^* < a^{\max} \text{ with } \frac{\bar{A}_i(a^*)}{k_{eq}(a^*)^2} = \frac{L_i^c}{h}, \\ d^* = h \sqrt{\frac{G_i^c}{E_i h \bar{A}_i(a^*)}} \\ L_i^c \geq L_i^{\max}, a^* = a^{\max}, d^* = h \sqrt{\frac{G_i^c}{E_i h \bar{A}_i(a^{\max})}} \end{cases} \quad (14)$$

It is to be noted that a^{\max} and L_i^{\max} are structural values which depend on the geometry. For $h = 2\text{mm}$, it is found that $a^{\max}/h = 0.09$ and $L_i^{\max}/h = 0.87$. Numerical results (obtained for $0.5\text{mm} \leq h \leq 2\text{mm}$) reveal that these values are weakly dependent on h . Relation (14) is illustrated in Fig. 4a which plots the crack length at initiation versus the ratio $\frac{L_i^c}{h}$. Figure 4b plots the predicted applied displacement at initiation of debonding versus $\frac{L_i^c}{h}$ for two values of the interfacial strength. As expected this critical displacement increases with L_i^c for a given value of σ_i^c (or equivalently with G_i^c for a given value of σ_i^c).

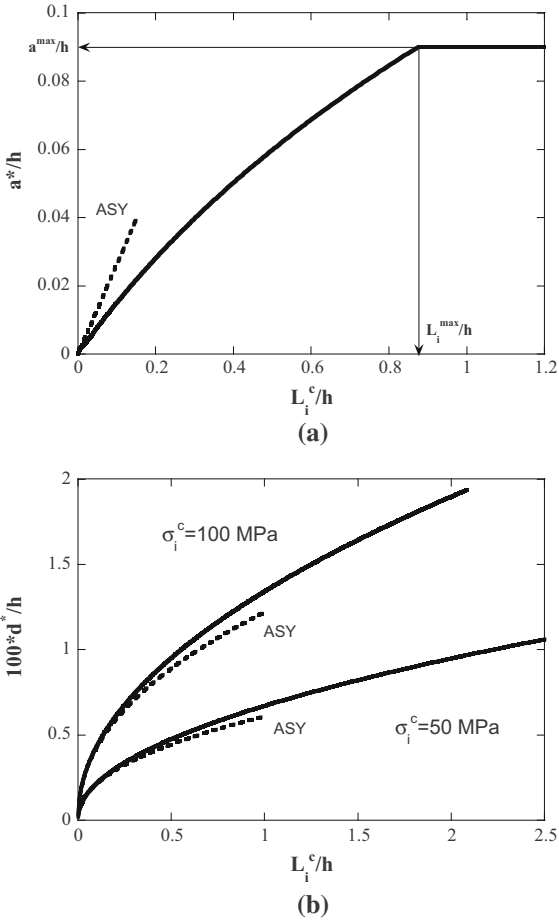


Fig. 4 Predictions provided by the coupled criterion: **a** crack length at initiation of debonding versus the characteristic fracture length of the interface, **b** applied displacement at initiation of debonding versus the characteristic fracture length of the interface for two values of the interfacial strength; the values provided by the asymptotic analysis (ASY) are also plotted with *dotted lines* and are explained in the next section

2.2 Comparison with the asymptotic approach

It is interesting to compare the presented approach which relies on direct finite element computations with the asymptotic expansion procedure proposed by Leguillon and Sanchez-Palencia (1987). The theory of singularity allows expressing the tensile stress σ_{yy} along the interface in the vicinity of the edge by

$$\sigma_{yy}(x) = E_i k_0 \left(\frac{x}{h}\right)^{\lambda-1} \left(\frac{d}{h}\right), \quad (15)$$

where the singularity exponent is $\lambda = 0.545$ (Leguillon et al. 2003). The dimensionless coefficient k_0 is related to the generalized stress intensity factor and can be

computed using a path independent integral (Leguillon and Sanchez-Palencia 1992).

The incremental energy release rate is given by

$$G_i^{inc}(a) = E_i h A_0 \left(\frac{a}{h}\right)^{2\lambda-1} \left(\frac{d}{h}\right)^2. \quad (16)$$

Determining the scaling coefficient A_0 requires matching asymptotic expansions and the use of a path independent integral (Leguillon and Sanchez-Palencia 1992). The coefficients k_0 and A_0 do not depend on the thickness h . Combining (15) and (16) with the stress and energy conditions required by the CC takes advantage to provide analytical expressions for crack length and displacement at crack initiation by

$$\begin{cases} a^* = \left(\frac{k_0^2}{A_0}\right) L_i^c \\ d^* = h \left(\frac{G_i^c}{E_i A_0 h}\right)^{1-\lambda} \left(\frac{\sigma_i^c}{E_i k_0}\right)^{2\lambda-1} \end{cases} \quad (17)$$

As expected from the asymptotic assumption, Fig. 4a reveals that equations (14) and (17) only match for small values of the characteristic length such that $L_i^c < 0.05h$, i.e. L_i^c must be small compared to the characteristic dimension of the structure. This condition thus implies small initiation lengths for which the asymptotic analysis is valid. In this case, the initiation length is proportional to L_i^c as shown by (17). Figure 4b indicates that using (17) for larger values of L_i^c ($L_i^c \geq 0.1h$) leads to underestimate the load at initiation. In this case, the approximation $a^* = a^{\max}$ in (14) produces a reliable estimate of d^* as a consequence of the slow variation of $\bar{A}_i(a)$ with a .

2.3 Propagation of the interfacial crack

Even if we focus on the initiation of the interfacial crack, the analysis of its subsequent propagation is worthwhile for comparison purpose. The usual Griffith criterion requires

$$G_i(a) = -\frac{1}{b} \frac{dW}{da} \geq G_i^c \quad \text{and} \quad a \geq a^*. \quad (18)$$

The differential energy release rate $G_i(a)$ is expressed as

$$G_i(a) = E_i h A_i(a) \left(\frac{d}{h}\right)^2, \quad (19)$$

where $A_i(a)$ is a dimensionless coefficient. As a consequence of (3), the relationship between the dimensionless coefficients $\bar{A}_i(a)$ and $A_i(a)$ is given by

$$\bar{A}_i(a) = \frac{1}{a} \int_0^a A_i(\ell) d\ell. \quad (20)$$

Reminding that the incremental energy release rate is maximum for $a = a^{\max}$ allows writing

$$\frac{d\bar{A}_i}{da}(a = a^{\max}) = 0. \quad (21)$$

As shown by (Martin and Leguillon 2004), combining (20) and (21) leads to

$$\bar{A}_i(a^{\max}) = A_i(a^{\max}). \quad (22)$$

Figure 3 plots the evolution of A_i and \bar{A}_i versus the crack length, it illustrates this last relation and also discloses that

$$A_i(a) > \bar{A}_i(a) \text{ for } a < a^{\max}. \quad (23)$$

Once $G_i(a)$ is estimated, applying the Griffith criterion provides the crack length a (d) versus the applied displacement as depicted by Fig. 5a for $\sigma_i^c = 500$ MPa. This plot clearly reveals a crack jump at initiation of debonding. For high values of the characteristic length such that $L_i^c \geq L_i^{\max}$, the nucleation length is $a^* = a^{\max}$ with $G^{inc}(a^*) = G_i(a^*) = G_i^c$ which shows that a^* is an arrest length. This is the case in Fig. 5a for $G_i^c = 2500 \text{ Jm}^{-2}$ which leads to $L_i^c = 2.08h \geq L_i^{\max}$. Reducing L_i^c with $L_i^c < L_i^{\max}$ implies $a^* < a^{\max}$ and $G_i(a^*) > G^{inc}(a^*) = G_i^c$ as a consequence of (23). The nucleated crack is thus unstable and reaches the length a_1 defined by $G_i(a_1) = G_i^c$ with $a_1 > a^{\max}$ as it is observed in Fig. 5a for $G_i^c = 100, 500, 1000 \text{ Jm}^{-2}$. Evaluating the compliance $C(a)$ of the specimen versus the interfacial crack length supplies the applied force $F = \frac{d}{C(a(d))}$ as plotted in Fig. 5b. This figure identifies the applied load at initiation of debonding and shows the corresponding decrease of the load which is followed by a stable crack propagation.

3 Cohesive zone model

A cohesive zone model is defined by surface constitutive relations which describe the evolution of tractions $[T]$ generated across the faces of a process zone as a function of the relative opening $[u]$. Among the various two-dimensional shapes of the model which have been proposed (Alfano 2006), we select a bilinear law (Alfano and Crisfield 2001) which writes

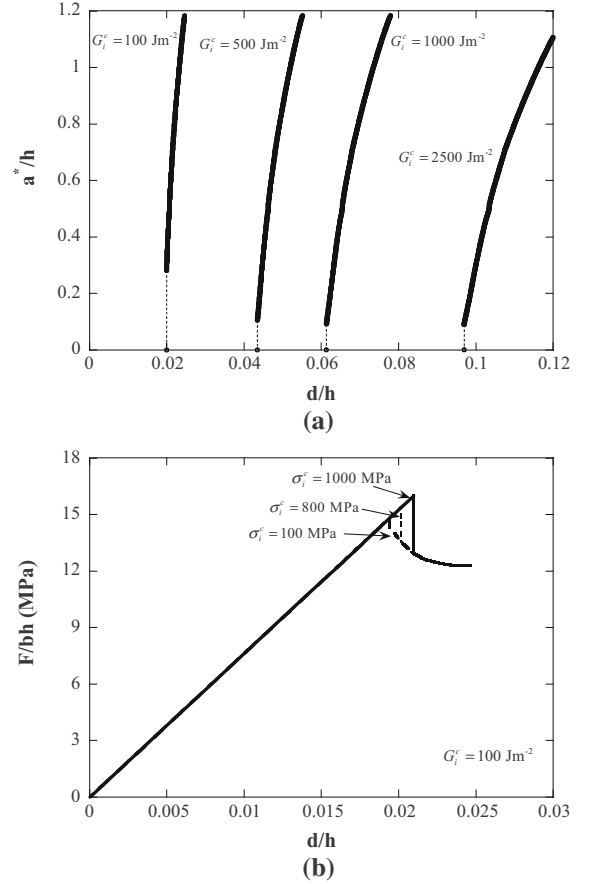


Fig. 5 Predictions provided by the coupled criterion: **a** crack length versus the applied displacement for $\sigma_i^c = 500$ MPa and various values of G_i^c , **b** load-displacement curve for $G_i^c = 100 \text{ Jm}^{-2}$ and various values of σ_i^c

$$\begin{cases} T_n = (1 - \beta) \frac{u_n}{\delta_{0n}} \sigma_i^c \\ T_t = (1 - \beta) \frac{u_t}{\delta_{0t}} \tau_i^c \end{cases}, \quad (24)$$

where $[T] = (T_n, T_t)$ are respectively the normal and tangential interfacial tractions and $[u] = (u_n, u_t)$ are respectively the normal and tangential relative displacements along the interface. The traction-separation law is linear and reversible prior to the peak traction. During the softening phase, the damage variable is $\beta = \frac{\kappa}{\eta(1+\kappa)}$ with $\eta = \left(1 - \frac{\delta_{0n}}{\delta_n^c}\right) = \left(1 - \frac{\delta_{0t}}{\delta_t^c}\right)$ and $\kappa = \sqrt{\left(\frac{u_n}{\delta_{0t}}\right)^2 + \left(\frac{u_t}{\delta_{0n}}\right)^2} - 1$. No attempt was made here to distinguish mode I from mode II by setting $\sigma_i^c = \tau_i^c$, $\delta_{0n} = \delta_{0t} = \delta_0$ and $\delta_n^c = \delta_t^c = \delta^c$. This specific choice implies that i) the initiation of interfacial damage is driven by a stress criterion similar to condition (8), ii)

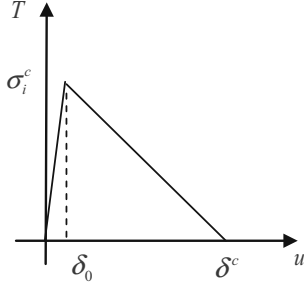


Fig. 6 Traction-separation law of the bilinear cohesive zone model

the propagation of damage depends on the interfacial fracture energy $G_i^c = \frac{1}{2}\sigma_i^c\delta^c$ whatever the mode mix. The CZM is thus defined with the help of the three parameters $(\delta_0, \delta^c, \sigma_i^c)$ as plotted in Fig. 6.

A small value of the separation threshold $\frac{\delta_0}{h} = 5 \cdot 10^{-6}$ is chosen. With such a choice, the overall rigidity of the model and the computational convergence are not altered. Practical use of a CZM requires a mesh fine enough to obtain an accurate resolution of the cohesive length. This condition can be expressed with the help of an upper bound of the mesh size defined by $L_{mesh} \leq \frac{1}{3}L_{czm}$ with $L_{czm} \approx \frac{\pi}{2}L_i^c$ (Acary and Monerie 2006). Another requirement states that the critical displacement δ^c must be smaller than the characteristic dimension of the structure which can be formulated as $\delta^c < \frac{h}{10}$. Reminding that $G_i^c = \frac{1}{2}\sigma_i^c\delta^c$, this condition establishes an upper bound of L_i^c for a given value of the interfacial strength. Finally, these two conditions lead to

$$\frac{6}{\pi} \frac{L_{mesh}}{h} < \frac{L_i^c}{h} < \frac{1}{20} \frac{E_i}{\sigma_i^c}. \quad (25)$$

To analyze the mechanical behavior of the bimaterial specimen (Fig. 1), cohesive zone elements are inserted at the interface between the two substrates. The parameters of the CZM are selected in order to satisfy condition (25). An implicit quasi-static finite element code (Burllet and Cailletaud 1991) is used to perform the analysis. A large number of loading increments is imposed to capture accurately the applied loading at crack onset. The crack length is recorded by tracking the interfacial elements for which the damage variable reaches the value $\beta = 1$. Figure 7 plots some predictions provided by the bilinear CZM. A peak force (Fig. 7b) is recorded on the load displacement curve which indicates initiation of edge debonding which is

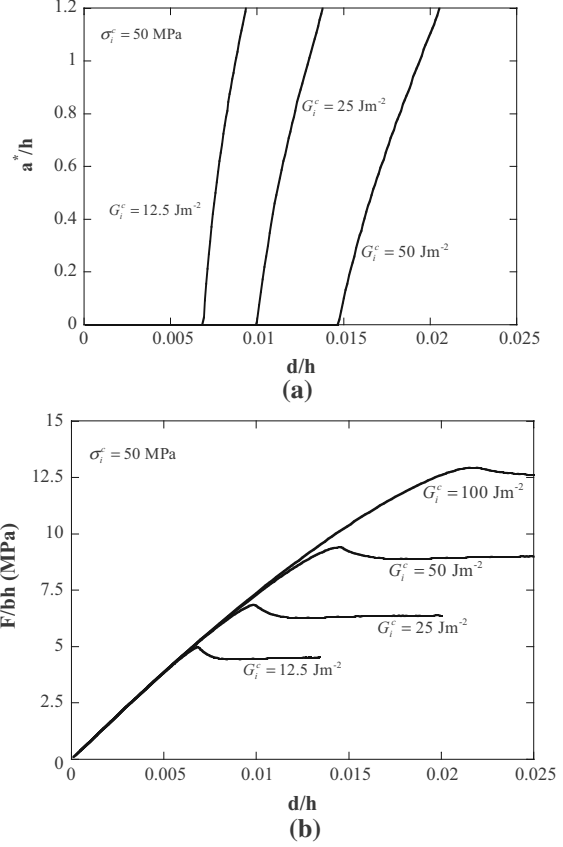


Fig. 7 Predictions provided by the bilinear CZM : **a** crack length and **b** load-displacement curve versus the applied displacement for $\sigma_i^c = 50$ MPa and various values of G_i^c

followed by crack propagation (Fig. 7a). The softening part observed on the load displacement response results from the development of the cohesive zone (or interfacial damage also called process zone) prior to crack initiation.

4 Results and discussion

A series of finite element computations was performed to compare the applied displacement for the onset of interfacial cracking as provided by the CC and CZM. Figure 8 reveals that a good agreement is only obtained with the smallest values of the fracture length such that $\frac{L_i^c}{h} < 1$. This result was already observed by previous authors (Henninger et al. 2007; Murer and Leguillon 2010) showing a perfect agreement between the coupled criterion and the Dugdale cohesive zone model with a rectangular shape for predicting crack initiation

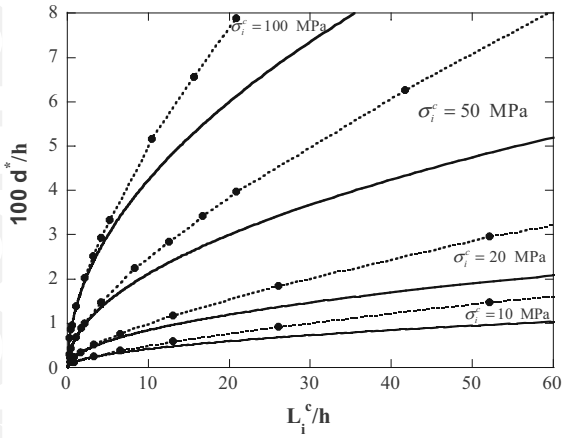


Fig. 8 Comparison between CC (solid lines) and CZM (dotted lines): prediction of applied displacement at initiation of debonding versus the characteristic fracture length of the interface for different values of the interfacial strength

at a V notch : these comparisons were carried out within an asymptotic framework which assumes small crack increments and thus small fracture lengths.

In order to analyze these results, force and crack length are now examined as a function of the applied displacement. Figure 9a shows that the response of the CZM is very close to the response provided by the finite fracture mechanics approach for $\frac{L_i^c}{h} = 1.042$. In this case, CZM produces a small cohesive length and can match the brittle response of the CC. Increasing the fracture length with $\frac{L_i^c}{h} = 10.42$ extends the cohesive zone and induces a large amount of softening which postpones crack onset (Fig. 9b). In this case, the damageable response of the CZM is enhanced and moves away from the brittle response of the CC. This draws the conclusion that CZM cannot reproduce a brittle interfacial behavior with a large fracture length.

Previous authors (Acary and Monerie 2006) have pointed out that the shape of the cohesive law influences the crack initiation. This is confirmed by a previous work (Vandellos et al. 2014) comparing different shapes of CZM defined within the framework proposed by (Vandellos et al. 2013). Those results indicate that the trapezoidal CZM provides results closer to those obtained with the CC when compared with the bilinear shape. This result is directly related to the observation that the cohesive length of the trapezoidal shape is smaller than the bilinear one.

Both approaches (CC and CZM) are now used to analyze an experimental response. Our aim here is to

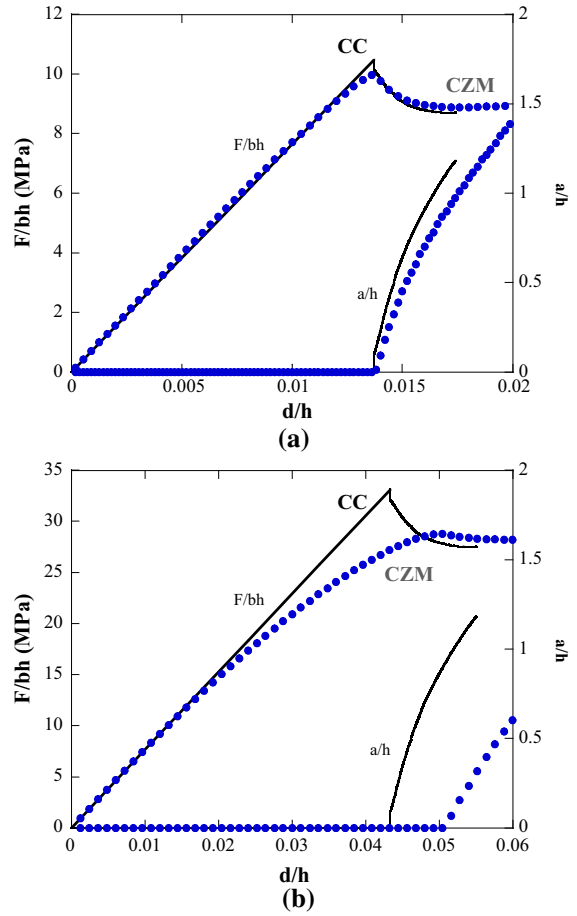


Fig. 9 Comparison between the load-displacement and crack-displacement response predicted by CC and bilinear CZM: **a** $\sigma_i^c = 100$ MPa, $G_i^c = 50$ Jm⁻², **b** $\sigma_i^c = 100$ MPa, $G_i^c = 500$ Jm⁻²

illustrate the difference between CC and CZM and also to show that they can be complementary. For this purpose, a testing result demonstrating interfacial damage is selected. The specimen (with the geometry already given in section 1) consists in two silicon carbide substrates bonded by a porous interlayer with the help of a sintering process (Jacques et al. 2014). The elastic properties of the substrate are $E_s = 420$ GPa and $\nu_s = 0.14$. The thickness of the interlayer is $e = 0.3$ mm and the width of the sample is $b = 4$ mm. A contacting transducer was used to estimate the specimen deflection at mid span. Depending on the bond strength (controlled by the sintering conditions as shown by Jacques (2012)), experimental results have evidenced substrate cracking or edge debonding. Substrate cracking can be easily analyzed with CC (Martin et al. 2014) and

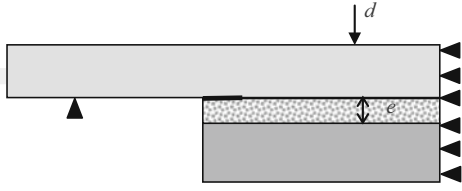


Fig. 10 Geometry of the two-dimensional model with an interlayer; edge debonding is introduced at the upper edge of the substrate/interlayer interface

we focus on the last case which exhibits the typical mechanical response plotted in Fig. 11. This response reveals a non-linear part which results from the damage of the weak interlayer followed by a plateau which corresponds to the interfacial crack propagation (Jacques 2012). According to the previous results, it is clear that the CC is not able to reproduce the observed softening but it is used to provide a first estimate of the interfacial parameters needed by the CZM.

The finite fracture mechanics approach is first undertaken. The two-dimensional model (Fig. 10) now includes the interlayer whose thickness cannot be considered as negligible when compared to the substrates one. Following the guidelines recommended by previous authors (Moradi et al. 2013b), at least twenty elements are inserted within the interlayer thickness. It is also assumed that edge debonding occurs at the upper edge of the substrate/interlayer interface where the stress singularity is maximum (Moradi et al. 2013a).

The comparison of the initial slope of the experimental response with the finite element results provides an estimate of the modulus of the porous interlayer ($E_{layer} = 2$ GPa) and it is assumed that $\nu_{layer} = 0.2$. As depicted in Fig. 11, the experimental response exhibits a plateau corresponding to the interfacial propagation. This stable step allows one to estimate the interfacial fracture energy with the help of relation (18) and leads to $G_i^c = 28 \text{ Jm}^{-2}$. The value of the structural length L_i^{\max} is found to be $L_i^{\max} = 28.13 \text{ h}$. Satisfying (12) thus implies that the interfacial strength σ_i^c must be lower than $\sigma_i^* = 14.7 \text{ MPa}$ to obtain a dominant energy condition. Assuming a weak enough interlayer, this condition leads to the prediction plotted in Fig. 11a which does not depend on σ_i^c . Increasing the estimation of σ_i^c over σ_i^* will increase the applied displacement and load at initiation of debonding as already displayed in Fig. 5b and will move away the prediction from the experimental response. It is clear that the CC hypo-

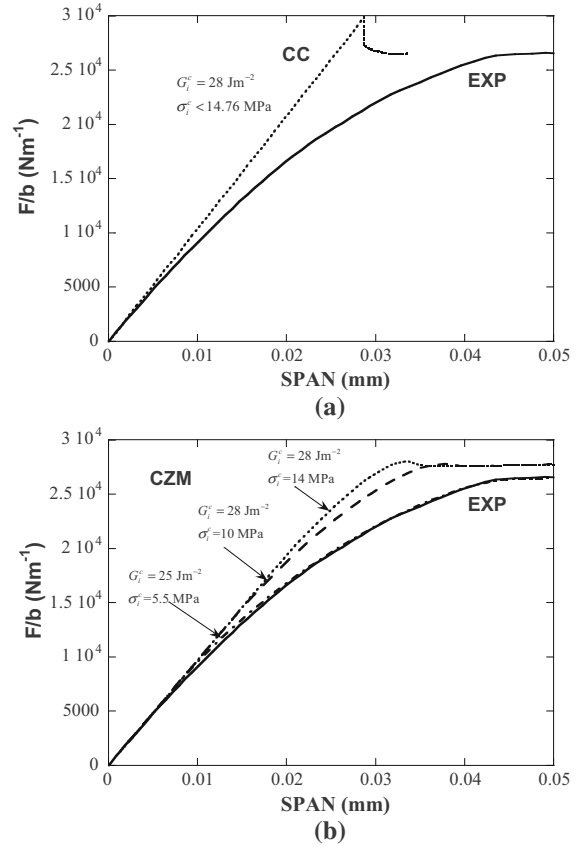


Fig. 11 Comparison between the experimental load-span response of a bonded specimen with **a** the CC prediction, **b** the bilinear CZM prediction

esizes a finite crack increment at initiation and cannot reproduce the non-linearity observed on the experimental response. Nevertheless, the FFM approach easily provides a first estimate of the interfacial fracture properties.

The bilinear CZM is now used. In this case, the interlayer is not meshed but introduced by relating the parameter δ_0 to the interlayer modulus with $\delta_0 = e \frac{\sigma_i^c}{E_{layer}}$. The interfacial properties obtained with the help of the CC are first used and the results are plotted in Fig. 11b. The prediction based on $G_i^c = 28 \text{ Jm}^{-2}$ and $\sigma_i^c = 14 \text{ MPa}$ is not close to the response provided by the CC. According to the results of the comparison between CZM and CC presented in Fig. 8, this was expected because the value of $\frac{L_i^c}{h} = 26.9$ is significantly larger than unity. The plateau value is also higher. Reducing σ_i^c to a value of 10 MPa decreases the non-linearity threshold. This is clearly different from

the CC prediction which is independent from σ_i^c for $\sigma_i^c \leq \sigma_i^* = 14.7$ MPa. Finally a good agreement with the experimental response is found for $G_i^c = 25$ Jm⁻² and $\sigma_i^c = 5.5$ MPa.

4.1 Conclusion

Initiation of edge debonding within a bimaterial specimen submitted to four point bending was predicted both using FFM and CZM. The first approach relies on the CC which combines a stress and an energy conditions. The CZM uses a bilinear interface law. The comparison between these approaches reveal their advantages and drawbacks : i) CC is limited to a brittle behavior (whatever the fracture length), ii) CZM only produces a linear response for small values of the fracture length and shifts to a non linear response for large values of the fracture length. A good agreement between the two methods is only obtained for small values of the fracture lengths such that $\frac{L_i^c}{h} < 1$. Use of CZM with largest fracture lengths extends the cohesive zone and thus introduces softening which postpones crack initiation compared to the CC. Finally, the analysis of a specimen bonded with a damageable interlayer shows that the CC can be helpful to provide a first set of values to identify the parameters of the CZM. Further work should include the influence of mode mix on the initiation of edge debonding which was not included in the present analysis. However, this influence is expected to be weak as a consequence of the prevailing opening mode at least for moderate values of the ratio $\frac{L_i^c}{h}$ which will lead to short crack lengths at initiation.

References

- Acary V, Monerie Y (2006) Nonsmooth fracture dynamics using a cohesive zone approach. Research Report RR-6032, INRIA
- Adams RD, Wake WC (1984) Structural adhesive joints in engineering. Elsevier, USA
- Alfano G (2006) On the influence of the shape of the interface law on the application of cohesive-zone models. *Compos Sci Technol* 66:723–730. doi:10.1016/j.compscitech.2004.12.024
- Alfano G, Crisfield MA (2001) Finite element interface models for the delamination analysis of laminated composites: mechanical and computational issues. *Int J Numer Methods Eng* 50:1701–1736
- Allix O, Ladeveze P (1992) Interlaminar interface modelling for the prediction of delamination. *Compos Struct* 22:235–242
- Allix O, Corigliano A (1996) Modeling and simulation of crack propagation in mixed-modes interlaminar fracture specimens. *Int J Fract* 77:111–140
- Banks-Sills L (2015) Interface fracture mechanics: theory and experiment. *Int J Fract* 191:131–146. doi:10.1007/s10704-015-9997-1
- Barenblatt GI (1959) The formation of equilibrium cracks during brittle fracture: general ideas and hypotheses. *Axially-symmetric Cracks PMM* 23:622–636
- Bertolini J, Castanié B, Barrau J-J, Navarro J-P (2009) Multi-level experimental and numerical analysis of composite stiffener debonding. Part 1: Non-specific specimen level. *Compos Struct* 90:381–391. doi:10.1016/j.compstruct.2009.04.001
- Burlet H, Cailletaud G (1991) Zebulon a finite element code for non-linear material behaviour. In: *Proceedings of the European conference on new advances in computational structural mechanics*, 2–5 April 1991, Giens, France
- Campilho RDSG, Banea MD, Neto JABP, da Silva LFM (2012) Modelling of single-lap joints using cohesive zone models: effect of the cohesive parameters on the output of the simulations. *J Adhes* 88:513–533. doi:10.1080/00218464.2012.660834
- Carpinteri A (1982) Notch sensitivity in fracture testing of aggregative materials. *Eng Fract Mech* 16:467–481
- Carpinteri A, Cornetti P, Pugno N et al (2008) A finite fracture mechanics approach to structures with sharp V-notches. *Eng Fract Mech* 75:1736–1752. doi:10.1016/j.engfracmech.2007.04.010
- Carrère N, Martin E, Leguillon D (2015) Comparison between models based on a coupled criterion for the prediction of the failure of adhesively bonded joints. *Eng Fract Mech* 138:185–201. doi:10.1016/j.engfracmech.2015.03.004
- Corigliano A (1993) Formulation, identification and use of interface models in the numerical analysis of composite delamination. *Int J Solids Struct* 30:2779–2811
- Cornetti P, Corrado M, Lorenzis LD, Carpinteri A (2015) An analytical cohesive crack modeling approach to the edge debonding failure of FRP-plated beams. *Int J Solids Struct* 53:92–106. doi:10.1016/j.ijsolstr.2014.10.017
- Cornetti P, Pugno N, Carpinteri A, Taylor D (2006) Finite fracture mechanics: a coupled stress and energy failure criterion. *Eng Fract Mech* 73:2021–2033. doi:10.1016/j.engfracmech.2006.03.010
- Cotton J, Grant JW, Jensen MK, Love BJ (2001) Analytical solutions to the shear strength of interfaces failing under flexure loading conditions. *Int J Adhes Adhes* 21:65–70
- Da Silva LFM, Campilho RDSG (2012) *Advances in numerical modelling of adhesive joints*. Springer, Berlin, pp 1–93. doi:10.1007/978-3-642-23608-2_1
- De Lorenzis L, Zavarise G (2009) Cohesive zone modeling of interfacial stresses in plated beams. *Int J Solids Struct* 46:4181–4191
- Dugdale DS (1960) Yielding of steel sheets containing slits. *J Mech Phys Solids* 8:100–104
- García IG, Leguillon D (2012) Mixed-mode crack initiation at a v-notch in presence of an adhesive joint. *Int J Solids Struct* 49:2138–2149. doi:10.1016/j.ijsolstr.2012.04.018
- García IG, Mantič V, Blázquez A, París F (2014) Transverse crack onset and growth in cross-ply laminates under tension: application of a coupled stress and energy criterion. *Int J*

- Solids Struct 51:3844–3856. doi:10.1016/j.ijsolstr.2014.06.015
- García IG, Mantič V, Graciani E (2015) Debonding at the fibre-matrix interface under remote transverse tension. One debond or two symmetric debonds? *Eur J Mech-A/Solids* 53:75–88. doi:10.1016/j.euromechsol.2015.02.007
- Gustafson PA, Waas AM (2009) The influence of adhesive constitutive parameters in cohesive zone finite element models of adhesively bonded joints. *Int J Solids Struct* 46:2201–2215. doi:10.1016/j.ijsolstr.2008.11.016
- Hashin Z (1996) Finite thermoelastic fracture criterion with application to laminate cracking analysis. *J Mech Phys Solids* 44:1129–1145
- Hebel J, Dieringer R, Becker W (2010) Modelling brittle crack formation at geometrical and material discontinuities using a finite fracture mechanics approach. *Eng Fract Mech* 77:3558–3572. doi:10.1016/j.engfracmech.2010.07.005
- Hell S, Weißgräber P, Felger J, Becker W (2014) A coupled stress and energy criterion for the assessment of crack initiation in single lap joints: A numerical approach. *Eng Fract Mech* 117:112–126. doi:10.1016/j.engfracmech.2014.01.012
- Henninger C, Leguillon D, Martin E (2007) Crack initiation at a V-notch—comparison between a brittle fracture criterion and the Dugdale cohesive model. *Comptes Rendus Mécanique* 335:388–393. doi:10.1016/j.crme.2007.05.018
- Jacques E (2012) PhD Thesis (in french). No 4620, University of Bordeaux
- Jacques E, Le Petitcorps Y, Maillé L, Lorrette C, Chaffron L (2014) Joining silicon carbide plates by titanium disilicide-based compound. *Powder Metall Metal Ceram* 52:606–611
- Leguillon D (2002) Strength or toughness? A criterion for crack onset at a notch. *Eur J Mech A/Solids* 21:61–72
- Leguillon D, Laurencin J, Dupeux M (2003) Failure initiation in an epoxy joint between two steel plates. *Eur J Mech-A/Solids* 22:509–524. doi:10.1016/S0997-7538(03)00066-4
- Leguillon D, Martin E (2012) The strengthening effect caused by an elastic contrast—part I: the bimaterial case. *Int J Fract* 179:157–167. doi:10.1007/s10704-012-9787-y
- Leguillon D, Martin E, Ševeček O, Bermejo R (2015) Application of the coupled stress-energy criterion to predict the fracture behaviour of layered ceramics designed with internal compressive stresses. *Eur J Mech-A/Solids* 54:94–104. doi:10.1016/j.euromechsol.2015.06.008
- Leguillon D, Sanchez-Palencia E (1987) Computation of singular solutions in elliptic problems and elasticity. Wiley, USA
- Leguillon D, Sanchez-Palencia E (1992) Fracture in heterogeneous materials, weak and strong singularities. In: Ladevèze P, Zienkiewicz O (eds) *Proceedings of the European conference on new advances in computational structural mechanics*. Elsevier, Amsterdam, pp 229–236
- Lenz J, Schwarz S, Schwickerath H et al (1995) Bond strength of metal-ceramic systems in three-point flexure bond test. *J Appl Biomater* 6:55–64
- Liljedahl CDM, Crocombe AD, Wahab MA, Ashcroft IA (2006) Damage modelling of adhesively bonded joints. *Int J Fract* 141:147–161. doi:10.1007/s10704-006-0072-9
- Mantič V (2009) Interface crack onset at a circular cylindrical inclusion under a remote transverse tension. Application of a coupled stress and energy criterion. *Int J Solids Struct* 46:1287–1304. doi:10.1016/j.ijsolstr.2008.10.036
- Martin E, Leguillon D (2004) Energetic conditions for interfacial failure in the vicinity of a matrix crack in brittle matrix composites. *Int J Solids Struct* 41:6937–6948. doi:10.1016/j.ijsolstr.2004.05.044
- Martin E, Leguillon D (2015) A strain energy density criterion for the initiation of edge debonding. *Theor Appl Fract Mech* 79:58–61. doi:10.1016/j.tafmec.2015.06.011
- Martin E, Leguillon D, Carrère N (2010) A twofold strength and toughness criterion for the onset of free-edge shear delamination in angle-ply laminates. *Int J Solids Struct* 47:1297–1305. doi:10.1016/j.ijsolstr.2010.01.018
- Martin E, Leguillon D, Carrère N (2012) A coupled strength and toughness criterion for the prediction of the open hole tensile strength of a composite plate. *Int J Solids Struct* 49:3915–3922. doi:10.1016/j.ijsolstr.2012.08.020
- Martin E, Poitou B, Leguillon D, Gatt JM (2008) Competition between deflection and penetration at an interface in the vicinity of a main crack. *Int J Fract* 151:247–268. doi:10.1007/s10704-008-9228-0
- Martin E, Vandellos T, Leguillon D et al (2014) A finite fracture approach for determining the fracture onset of a brazed SiC specimen. *Proced Mater Sci* 3:129–134. doi:10.1016/j.mspro.2014.06.024
- Moradi A, Leguillon D, Carrère N (2013a) Influence of the adhesive thickness on a debonding - An asymptotic model. *Eng Fract Mech* 114:55–68. doi:10.1016/j.engfracmech.2013.10.008
- Moradi A, Carrère N, Leguillon D et al (2013b) Strength prediction of bonded assemblies using a coupled criterion under elastic assumptions: Effect of material and geometrical parameters. *Int J Adhes Adhes* 47:73–82. doi:10.1016/j.ijadhadh.2013.09.044
- Murer S, Leguillon D (2010) Static and fatigue failure of quasi-brittle materials at a V-notch using a Dugdale model. *Eur J Mech A Solids* 29:109–118. doi:10.1016/j.euromechsol.2009.10.005
- Nairn JA (2000) Exact and variational theorems for fracture mechanics of composites with residual stresses, traction-loaded cracks and imperfect interfaces. *Int J Fract* 105:243–271
- Sapora A, Cornetti P, Carpinteri A (2013) A finite fracture mechanics approach to V-notched elements subjected to mixed-mode loading. *Eng Fract Mech* 97:216–226. doi:10.1016/j.engfracmech.2012.11.006
- Schellekens JCJ, De Borst R (1993) A non-linear finite element approach for the analysis of mode-I free edge delamination in composites. *Int J Solids Struct* 30:1239–1253
- Turon A, Camanho PP, Costa J, Renart J (2010) Accurate simulation of delamination growth under mixed-mode loading using cohesive elements: Definition of interlaminar strengths and elastic stiffness. *Compos Struct* 92:1857–1864. doi:10.1016/j.compstruct.2010.01.012
- Tvergaard V, Hutchinson JW (1992) The relation between crack growth resistance and fracture process parameters in elastic-plastic solids. *J Mech Phys Solids* 40:1377–1397
- Vandellos T, Huchette C, Carrère N (2013) Proposition of a framework for the development of a cohesive zone model adapted to Carbon-Fiber Reinforced Plastic lam-

inated composites. *Compos Struct* 105:199–206. doi:10.1016/j.compstruct.2013.05.018

Vandellos T, Martin E, Leguillon D (2014) Comparison between Cohesive zone models and a coupled criterion for prediction of edge debonding, Proceedings of the 16th European Conference on Composite Materials, ECCM-16, 22–26 Jun 2014, Séville, Spain

Weißgraeber P, Becker W (2013) Finite Fracture Mechanics model for mixed mode fracture in adhesive joints. *Int J Solids Struct* 50:2383–2394. doi:10.1016/j.ijsolstr.2013.03.012

Xu X, Needleman A (1994) Numerical simulations of fast crack growth in brittle solids. *J Mech Phys Solids* 42:1397–1434